Membrane Translocation Mechanism of the Antimicrobial Peptide Buforin 2†

Satoe Kobayashi,§ Akinori Chikushi,‡ Shiho Tougu,§ Yuichi Imura,‡ Minoru Nishida,‡ Yoshiaki Yano,§ and Katsumi Matsuzaki*,§

Graduate School of Pharmaceutical Sciences and Graduate School of Biostudies, Kyoto University, Sakyo-ku, Kyoto 606-8501, Japan

Received August 19, 2004; Revised Manuscript Received September 26, 2004

ABSTRACT: The antimicrobial peptide magainin 2 isolated from the skin of the African clawed frog *Xenopus laevis* crosses lipid bilayers by transiently forming a peptide−lipid supramolecular complex pore inducing membrane permeabilization and flip-flop of membrane lipids [Matsuzaki, K., Murase, O., Fujii, N., and Miyajima, K. (1996) *Biochemistry 35*, 11361−11368]. In contrast, the antimicrobial peptide buforin 2 discovered in the stomach tissue of the Asian toad *Bufo bufo gargarizans* efficiently crosses lipid bilayers without inducing severe membrane permeabilization or lipid flip-flop, and the Pro^{11} residue plays a key role in this unique property [Kobayashi, S, Takeshima, K., Park, C. B., Kim, S. C., and Matsuzaki, K. (2000) *Biochemistry 39*, 8648−8654]. To elucidate the translocation mechanism, the secondary structure and the orientation of the peptide in lipid bilayers as well as the effects of the peptide concentration, the lipid composition, and the cis−trans isomerization of the Pro peptide bond on translocation efficiency were investigated. The translocation efficiencies of F10W-buforin 2 (BF2), P11A-BF2, and F5W-magainin 2 (MG2) across egg yolk L-α-phosphatidyl-DL-glycerol (EYPG)/egg yolk L-α-phosphatidylcholine (1/1) bilayers were dependent supralinearly on the peptide concentration, suggesting that the translocation mechanisms of these peptides are similar. The incorporation of the negative curvature-inducing lipid egg yolk L-α -phosphatidylethanolamine completely suppressed the translocation of BF2, indicating the induction of the positive curvature by BF2 on the membrane is related to the translocation process, similarly to MG2. In pure EYPG, where the repulsion between polycationic BF2 molecules is reduced, membrane permeabilization and coupling lipid flip-flop were clearly observed. Structural studies by use of Fourier transform infrared-polarized attenuated total reflection spectroscopy indicated that BF2 assumed distorted helical structures in EYPG/EYPC bilayers. A BF2 analogue with an α-methylproline, which fixed the peptide bond to the trans configuration, translocated similarly to the parent peptide, suggesting the cis−trans isomerization of the Pro peptide bond is not involved in the translocation process. These results indicate that BF2 crosses lipid bilayers via a mechanism similar to that of MG2. The presence of Pro^{11} distorts the helix, concentrating basic amino acid residues in a limited amphipathic region, thus destabilizing the pore by enhanced electrostatic repulsion, enabling efficient translocation.

Several hundred polycationic antimicrobial peptides have been discovered in both the animal and the plant kingdoms, and many are promising candidates for novel antibiotics (*1*−*4*). Most peptides have been considered to kill bacteria by permeabilizing negatively charged bacterial membranes, although accumulating evidence suggests that even these membrane-active peptides have multiple targets including intracellular components, such as DNA (*2*). A representative peptide of this class is magainin 2 isolated from the skin of the African clawed frog *Xenopus laevis* (Table 1) (*5*−*7*). The following mechanisms have been proposed for membrane permeabilization induced by these peptides. The peptide forms an amphipathic helix in lipid bilayers, which essentially lies parallel to the membrane surface (*8*, *9*), imposing a positive curvature strain on the membrane (*10*,

Table 1: Amino Acid Sequences of the Peptides Used

peptide	sequence
MG2 (F5W-magainin 2)	GIGKWLHSAKKFGKAFVGEIMNS
BF2 (F10W-buforin 2)	TRSSRAGLQWPVGRVHRLLRK
P11A-BF2 (F10W, P11A-buforin 2)	TRSSRAGLQWAVGRVHRLLRK
DNS-BF2	dansyl-TRSSRAGLQFPVGRVHRLLRK
DNS-MePro-BF2[a]	dansyl-TRSSRAGLQF-MeP-VGRVHRLLRK

[a] MeP: α-methylproline.

† Supported in part by the Grant-in-Aid for Scientific Research (14572091) from the Ministry of Education, Culture, Sports, Science and Technology of Japan.

* To whom correspondence should be addressed. Telephone: 81-75-753-4521. Fax: 81-75-753-4578. E-mail: katsumim@pharm.kyoto-u.ac.jp.

§ Graduate School of Pharmaceutical Sciences, Kyoto University.

‡ Graduate School of Biostudies, Kyoto University.

[1] Abbreviations: ANTS, 8-aminonaphthalene-1,3,6-trisulfonic acid, disodium salt; C_6-NBD-PC, 1-palmitoyl-2-[6-((7-nitrobenz-2-oxa-1,3-diazol-4-yl)amino)caproyl]-L-α-phosphatidylcholine; DNS-PE, *N*-[[(5-(dimethylamino)naphthyl)-1-sulfonyl] egg yolk L-α-phosphatidylethanolamine; DPX, *p*-xylene-bis-pyridinium bromide; EYPC, egg yolk L-α-phosphatidylcholine; EYPE, egg yolk L-α -phosphatidylethanolamine; EYPG, L-α-phosphatidyl-DL-glycerol enzymatically converted from EYPC; FRET, fluorescence resonance energy transfer; FTIR-PATR, Fourier transform infrared-polarized attenuated total reflection; LUVs, large unilamellar vesicles; MLVs, multilamellar vesicles; P/L, peptide-to-lipid molar ratio.

10.1021/bi048206q CCC: $27.50
Published on Web 11/17/2004

11). Several helices together with several surrounding lipids then form a membrane-spanning pore comprising a dynamic, peptide-lipid supramolecular complex (toroidal pore), which allows not only ion transport but also rapid flip-flop of the membrane lipids (*12*, *13*). Upon disintegration of the pore, a fraction of the peptide molecules stochastically translocate into the inner leaflet (*14*).

In contrast to these membrane-active peptides, other classes of antimicrobial peptides are suggested to target bacterial components other than membranes. Buforin 2 discovered in the stomach tissue of the Asian toad *Bufo bufo gargarizans* is one example (*15*) (Table 1). This peptide efficiently crosses lipid bilayers without inducing severe membrane permeabilization or lipid flip-flop (*16*). Furthermore, the peptide also crosses biological membranes and strongly binds to DNA and RNA (*17*, *18*), although the mechanism is yet to be elucidated.

In this study, to elucidate the translocation mechanism of buforin 2, we investigated the interactions of several buforin analogues with lipid bilayers in comparison with a magainin analogue (Table 1). We found that buforin crosses membranes via a mechanism similar to that of magainin 2, i.e., pore formation, and that the extremely short lifetime of the pore allows the peptide to translocate without membrane permeabilization.

MATERIALS AND METHODS

Materials. The peptides used in this study (Table 1) were custom synthesized and characterized by Peptide Institute (Minou, Japan). The purities were greater than 95% as determined by high-performance liquid chromatography. Trp residues were introduced to fluorometrically monitor peptide−membrane interactions. These derivatives have been confirmed to be equipotent to the parent peptides (*9*, *16*). Egg yolk L-α-phosphatidylcholine (EYPC), L-α-phosphatidyl-DL-glycerol enzymatically converted from EYPC (EYPG), and egg yolk L-α -phosphatidylethanolamine (EYPE) were obtained from Sigma (St. Louis, MO). 1-Palmitoyl-2-[6-((7-nitrobenz-2-oxa-1,3-diazol-4-yl)amino)caproyl]-L-α-phosphatidylcholine (C_6-NBD-PC) and *N*-[[(5-(dimethylamino)-naphthyl)-1-sulfonyl] egg yolk L-α-phosphatidylethanolamine (DNS-PE) were purchased from Avanti Polar Lipids (Alabaster, AL). 8-Aminonaphthalene-1,3,6-trisulfonic acid, disodium salt (ANTS), and *p*-xylene-bis-pyridinium bromide (DPX) were obtained from Molecular Probes (Eugene, OR). All other chemicals were of special grade and were supplied by Wako (Tokyo, Japan).

Lipid Vesicles. Large unilamellar vesicles (LUVs) were prepared and characterized as described elsewhere (*12*). Briefly, a lipid film, after drying under vacuum overnight, was hydrated with the desired solution and vortex-mixed to produce multilamellar vesicles (MLVs). The suspension was subjected to five freeze−thaw cycles and then extruded through polycarbonate filters (100 nm pore size filter, 21 times). The lipid concentration was determined in triplicate by phosphorus analysis (*19*).

Translocation. For Trp-containing peptides, a lipid film (EYPC/EYPG/DNS-PE = 50/45/5) was hydrated with a 0.2 mM trypsin solution in a 10 mM HEPES/45 mM NaCl/1 mM EDTA buffer (pH 7.4), and LUVs were prepared. Trypsin-chymotrypsin inhibitor (2 mM) was added to the same volume of LUV suspension to inactivate the enzyme outside the vesicles. Aliquots of the LUV suspension were injected into the peptide solution while monitoring the sensitized dansyl fluorescence intensity at 512 nm (excitation at 285 nm). A decrease in fluorescence implied digestion of the fluorescent peptide by the enzyme within the liposomes, i.e., internalization of the peptide. For the control experiments, LUVs in which the enzyme inhibitor was also encapsulated were used. The concentrations of trypsin and the inhibitor inside the LUVs were 0.2 and 2 mM, respectively. For dansylated peptides, the lipid composition was EYPG/EYPC/C_6-NBD-PC = 50/45/5, and fluorescence was monitored at 448 nm (excitation at 328 nm).

ANTS/DPX Leakage. An EYPG film was hydrated with a 6 mM ANTS/24 mM DPX/10 mM HEPES/45 mM NaCl/1 mM EDTA (pH 7.4) buffer, and LUVs were prepared. Immediately after the extrusion, vesicles containing ANTS/DPX were separated from free ANTS and DPX on a Biogel A-1.5m column. The release of ANTS and/or DPX from the LUVs was fluorometrically monitored on a Shimadzu RF-5000 spectrofluorometer at an excitation wavelength of 353 nm and an emission wavelength of 520 nm. The maximum fluorescence intensity corresponding to 100% leakage was determined by the addition of 10% w/v Triton X-100 (20 μL) to 2 mL of the sample. The apparent percent leakage value was calculated according to eq 1.

$$\%\ \text{apparent leakage} = 100 \times (F - F_0)/(F_t - F_0) \quad (1)$$

F and F_t denote fluorescence intensities before and after the addition of detergent, respectively. F_0 represents fluorescence of intact vesicles. Ladokhin et al. described the details of the ANTS/DPX leakage experiments (*20*).

Flip-Flop. The peptide-induced lipid flip-flop was detected as previously reported (*12*). NBD-labeled LUVs were generated from EYPG containing 0.5 mol % C_6-NBD-PC. The symmetrically labeled vesicles were mixed with 1 M sodium dithionite/1 M Tris ([lipid] = 40 mM, [dithionite] = 60 mM) and incubated for 15 min at 30 °C to produce inner leaflet-labeled vesicles. The vesicles were immediately separated from dithionite by gel-filtration (Bio-gel A1.5m, 1.5 × 30 cm column). The fraction of NBD-lipids that had flopped during incubation in the absence or presence of the peptide was measured on the basis of fluorescence quenching by sodium dithionite. The asymmetrically NBD-labeled LUVs (2.0 mL) were incubated with or without the peptide for various periods at 30 °C. In the peptide-containing samples, 20 μL of a trypsin solution (5 mg/mL) was added to 2 mL samples, and reacted for 1 min to hydrolyze the peptide. After addition of 20 μL of 1 M sodium dithionite/1 M Tris, NBD fluorescence was monitored with excitation and emission wavelengths of 460 and 530 nm, respectively. The percent flip-flop was calculated as described previously (*12*).

Fourier Transform Infrared-Polarized Attenuated Total Reflection (FTIR-PATR) Spectroscopy. Oriented films of EYPG/EYPC/peptide (20/20/1) were prepared by uniformly spreading a chloroform/methanol solution of the peptide−lipid mixture on a germanium ATR plate (80 × 10 × 4 mm) followed by gradual evaporation of the solvent. The last traces of the solvent were removed under vacuum overnight. The films were hydrated with a D_2O-soaked piece of filter

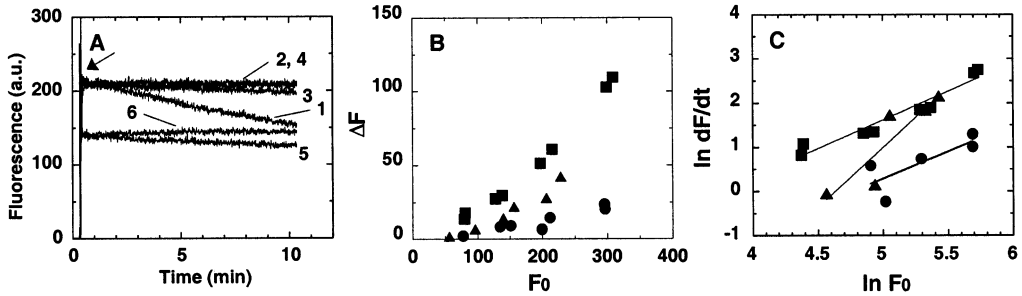

FIGURE 1: Translocation of BF2, P11A-BF2, and MG2 across EYPG/EYPC/DNS-PE (45/50/5) bilayers. (A) Aliquots of trypsin-entrapped LUV suspension were injected into peptide solution at the time indicated by the arrow while the sensitized dansyl fluorescence intensity was monitored at 512 nm (excitation at 285 nm). Indicated are fluorescence intensities after subtraction of blank fluorescence data in the absence of the peptides. For the control experiments (lines 2, 4, and 6), LUVs in which trypsin-chymotrypsin inhibitor was also encapsulated were used. The temperature was controlled at 30 °C. The final concentrations of the peptide and the lipid were 3 and 250 μM, respectively. Peptides: lines 1 and 2, BF2; lines 3 and 4, MG2; lines 5 and 6, P11A-BF2. (B) ΔF defined by the fluorescence intensity at the time of vesicle addition (F_0) minus the intensity after 9.9 min is plotted as a function F_0 for BF2 (squares), MG2 (circles), and P11A-BF2 (triangles). (C) Double logarithmic plots of the initial translocation rates $(dF/dt)_0$ from panel A versus F_0.

paper put over the plate for 3 h. The film thickness of about 6 μm, estimated from the applied amount of lipid, was much larger than the depth of penetration of the evanescent wave (0.2−0.8 μm) in the range 3000−800 cm^{-1}. To minimize spectral contributions of atmospheric water vapor, the instrument was purged with dry N_2 gas. FTIR-PATR measurements were carried out on a BioRad FTS-3000MX spectrometer equipped with a Hg-Cd-Te detector and a PIKE horizontal ATR attachment and a KRS-5 polarizer. The total reflection number was 10 on the film side. The spectra were measured at a resolution of 2 cm^{-1} and an angle of incidence of 45°, and derived from 256 co-added interferograms with the Happ-Genzel apodization function. The subtraction of the gently sloping water vapor was carried out to improve the background prior to frequency measurement. The dichroic ratio, R, defined by $\Delta A_{\parallel}/\Delta A_{\perp}$, was calculated from the polarized spectra. The absorbance (ΔA) was obtained as the area of each component band for the deconvolved amide I′ bands. The subscripts $\parallel$ and $\perp$ refer to polarized light with its electric vector parallel and perpendicular to the plane of incidence, respectively. For ATR correction, refractive indexes of 4.003 and 1.440 were used for germanium and the sample film, respectively (*21*). Deconvolution and curve-fitting of FTIR bands were performed by use of Peaksolve software (Thermo Galactic, Salem, NH). Deconvolution parameters of 25 cm^{-1} and 2.0 for the undeconvoluted band half-width and resolution enhancement factor, respectively, were used. Spectra were fitted with Gaussian band profiles. Unpolarized spectra, which were used to calculate the fraction of each component band, were obtained as a linear combination of polarized spectra (*22*).

RESULTS

Dose Dependence of Peptide Translocation. The translocation of the peptides across lipid bilayers was detected as reported elsewhere (*16*). Trypsin was encapsulated within the internal aqueous phase of EYPC/EYPG/DNS-PE (50/45/5) LUVs to selectively digest the translocated peptide. The enzyme outside the vesicles was inactivated by trypsin-chymotrypsin inhibitor. Fluorescence resonance energy transfer (FRET) from the Trp residues of the peptides to DNS-PE was utilized to monitor the membrane binding of the peptides, i.e., an increase in dansyl sensitized fluorescence at 512 nm when excited at 285 nm, where Trp is selectively excited. The enzyme hydrolyzes the peptide bonds on the C-terminal sides of the Lys and Arg residues. The hydrolyzed Trp-containing fragments will be desorbed from the membrane, resulting in relief of RET, i.e., a decrease in dansyl fluorescence. As shown in Figure 1A, the binding of the peptide to the vesicles abruptly increased dansyl fluorescence. The increased fluorescence was in the order BF2 (traces 1 and 2) = MG2 (traces 3 and 4) > P11A-BF2 (traces 5 and 6). BF2 (trace 1) crossed the membrane much more effectively than MG2 (trace 3). The translocation activity of P11A-BF2 was intermediate between those of BF2 and MG2 (trace 5). Traces 2, 4, and 6 indicate the control experiments in which the enzyme inhibitor was also present inside the vesicles. No digestion was observed. A closer inspection indicates that the dansyl fluorescence for P11A-BF2 (line 6) slightly increased with time, suggesting that the membrane binding of the peptide was incomplete and that upon translocation a part of the free peptide molecules bound to the outer leaflets in a time-dependent manner, as observed for model peptides (*23*).

The dose dependence of peptide translocation gives information on the translocation mechanism. Experiments similar to those in Figure 1A were carried out at peptide concentrations of 1, 2, 3, and 4 μM. The fluorescence intensity at the time of vesicle addition (F_0) is considered to be proportional to the concentration of the membrane-bound peptide. As a measure of the translocation efficiency, ΔF defined by F_0 minus the fluorescence intensity after 9.9 min was calculated and plotted as a function of F_0 (Figure 1B). For all peptides, ΔF was a higher order function of F_0, suggesting cooperativity. The slopes of the regression lines of the double logarithmic plots of Figure 1B were 1.4 ± 0.1 (R = 0.993), 1.6 ± 0.3 (R = 0.933), and 2.3 ± 0.1 (R = 0.994) for BF2, MG2, and P11A-BF2, respectively (plots not shown). We also estimated initial translocation rates $(dF/dt)_0$ from Figure 1A by the linear regressions of the initial parts of traces 1, 3, and 5. The $\ln[(dF/dt)_0]$ versus $\ln(F_0)$ plots (Figure 1C) gave similar slopes of 1.3 ± 0.7 (R = 0.968), 1.2 ± 0.6 (R = 0.782), and 2.7 ± 0.8 (R = 0.898) for BF2, MG2, and P11A-BF2, respectively.

Effects of Phosphatidylethanolamine. Translocation experiments were also carried out by substituting EYPE for EYPC. BF2 showed no translocation even at a high peptide concentration of 4 μM (data not shown). The F_0 value was

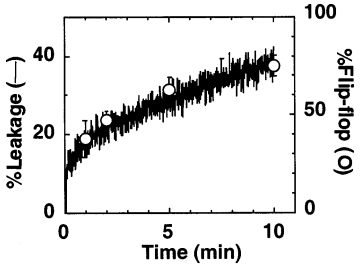

FIGURE 2: Coupling between dye leakage and lipid flip-flop induced by BF2 against EYPG LUVs at 30 °C. Time courses of ANTS/DPX leakage and lipid flip-flop are shown by lines and circles, respectively. Error bars show SD for two measurements. The final concentrations of the peptide and the lipid were 1 and 50 μM, respectively.

similar to that of Figure 1, indicating the membrane binding was not inhibited by the incorporation of EYPE.

Effects of Negative Charge Density. The above experiments were carried out using membranes containing 50% EYPG. An increase in membrane negative charge density would reduce repulsive interactions between the positively charged peptides in a putative peptide−lipid supramolecular complex pore, therefore stabilizing it. Figure 2 shows the pore formation of BF2 in pure EYPG LUVs at P/L = 1/50. Approximately 40% leakage of ANTS/DPX was observed for 10 min, whereas the peptide caused only 20% leakage against EYPG/EYPC LUVs (*16*). BF2 induced lipid flip-flop coupled to the dye leakage for EYPG LUVs (Figure 2), although the peptide did not induce detectable flip-flop for EYPG/EYPC LUVs (*16*).

Translocation experiments were also performed under the same conditions as Figure 2 (data not shown). The $\Delta F/F_0$ value was approximately 10%, whereas the value for EYPG/EYPC LUVs at a smaller P/L value of 1/63 was already as high as 40% (Figure 1B).

Effects of Trans−Cis Isomerization of Pro Peptide Bond. The peptide bond can take trans and cis configurations. In most cases, the trans form is energetically much favored. Proline is unique in that the side chain is bonded covalently to the nitrogen atom of the peptide backbone. The cyclic side chain diminishes repulsions between nonbonded atoms, and the intrinsic stability of the cis isomer is comparable to that of the trans isomer (*24*). The introduction of a methyl group at the C_α atom is known to fix the peptide bond in the trans form (*25*, *26*). To examine if the cis−trans isomerization is involved in the translocation of BF2, α-methylproline was substituted for Pro[11]. The F10W mutation was not carried out because the tenth position should be Phe to prepare a cis-fixed derivative (*27*). Instead the N terminus of the peptide was labeled by a dansyl group for monitoring peptide−lipid interactions (Table 1).

Translocation was detected in a manner similar to that outlined in Figure 1. The membrane was doped with C_6-NBD-PC, which serves as an FRET acceptor for the dansyl group, and the dansyl fluorescence was monitored. The binding of the peptide to the vesicles abruptly reduced dansyl fluorescence (Figure 3). A subsequent gradual increase implied digestion of the fluorescent peptide by the enzyme within the liposomes, i.e., internalization of the peptide. Both DNS-BF2 and DNS-MePro-BF2 showed almost identical translocation activities (upper two traces). For the control experiments, LUVs in which the enzyme inhibitor was also

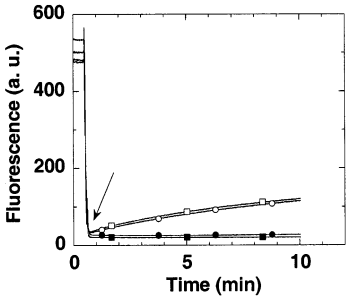

FIGURE 3: Translocation of DNS-BF2 and DNS-MePro-BF2 across EYPG/EYPC/C_6-NBD-PC (50/45/5) bilayers. Aliquots of trypsin-entrapped LUV suspension were injected into peptide solution at the time indicated by the arrow while the peptide dansyl fluorescence intensity was continuously monitored at 448 nm (excitation at 328 nm). Indicated are averaged fluorescence intensities (n = 2) after subtraction of blank fluorescence data in the absence of the peptide. The errors were within 5%. For the control experiments, LUVs in which 4 mM trypsin-chymotrypsin inhibitor was also encapsulated were used (closed symbols). The temperature was controlled at 30 °C. The final concentrations of the peptide and the lipid were 4 and 232 μM, respectively. Peptides: circles, DNS-BF2; squares, DNS-MePro-BF2.

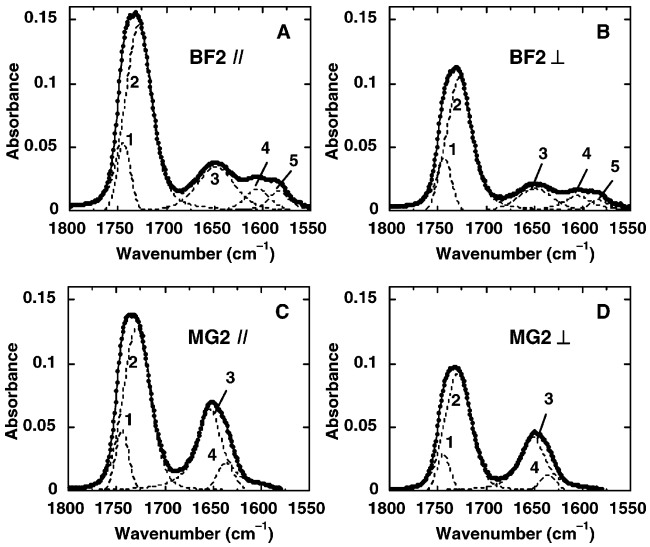

FIGURE 4: FTIR-PATR spectra of D_2O-hydrated films composed of peptide/EYPG/EYPC (1/20/20). Spectra of the amide I′ and carbonyl stretching region (small solid circles) were deconvolved into component bands (dotted lines). The sums (solid lines) of the resolved bands are superimposable to the observed spectra. Spectra for polarized light with its electric vector parallel (A and C) and perpendicular (B and D) to the plane of incidence are shown for BF2 (A and B) and MG2 (C and D).

encapsulated were used. No fluorescence increase was observed (lower two traces). The extent of translocation of DNS-BF2 during 10 min was ∼20%, which was comparable to that of BF2 (∼30%) under similar conditions (Figure 1B). Thus, the dansylated peptide mimics the parent peptide.

FTIR-PATR. Figure 4 shows the FTIR-PATR spectra of D_2O-hydrated films composed of peptide/EYPG/EYPC (1/20/20) in the amide I′ and carbonyl stretching region (1550−1800 cm^{-1}). The BF2 spectra (Figure 4A,B) could be deconvolved into five bands. Bands 1 and 2 centered at 1744 and 1729 cm^{-1}, respectively, were assigned to the stretching vibrations of the unhydrated and the monohydrated carbonyl groups of the lipids, respectively (*28*). The dichroic ratios of these bands were around 1.4 for all samples including pure lipid bilayers, indicating the membranes were well

Table 2: Conformations and Orientations of the Peptides in EYPG/EYPC (1/1) Bilayers

peptide	band[a]	wavenumber (cm^{-1})	R^b	α (°)
BF2	3	1649	2.1	51[c]
MG2	3	1651	1.5	74[c]
	4	1635	1.9	58[d]

[a] Peak number in Figure 4. [b] Dicroic ratio. Errors in duplicated experiments were within 0.1. [c] Angle between the helix axis and the membrane normal evaluated with eq 2 ($\theta = 35°$). [d] Angle between the amide I′ transition moment and the membrane normal evaluated with eq 2 ($\theta = 0°$).

oriented (*29*). Band 3 was assigned to the amide I′ band. Bands 4 and 5 centered at 1605 and 1583 cm^{-1}, respectively, were assigned to the asymmetric and symmetric stretching vibrations, respectively, of the $CN_3H_5^+$ groups of the Arg residues (*30*). The spectra of MG2 lacking Arg residues (Figure 4c,d) could be resolved into four bands. Two component bands (the bands 3 and 4) were observed in the amide I′ region.

The secondary structures and the orientations of the peptides can be estimated from the position and the dichroic ratio of the amide I′ band (*21*, *31*), which are summarized in Table 2. The wavenumbers of maximal intensity of the amide I′ bands of BF2 and MG2 (band 3) were 1649 and 1651 cm^{-1}, respectively, which are in the α-helix region. For MG2, the second component (band 4) comprising 13% of the total amide I′ intensity was centered at 1635 cm^{-1}, suggesting the presence of a β-strand conformation, as reported elsewhere (*32*).

The dichroic ratio can be used to determine the orientation of the transition dipoles, and therefore the molecular axis (*21*). Using the known angle, θ, between the molecular axis and the transition moments, the molecular orientation angle, α, around the membrane normal was calculated (*33*) and is summarized in Table 2.

$$\cos^2 \alpha = \frac{1}{3}\left(\frac{4}{3\cos^2 \theta - 1} \cdot \frac{R - 2.00}{R + 1.45} + 1\right) \qquad (2)$$

For the α-helical components, a θ value of 35° was used (*34*). For the β-strand component, a θ value of 0° was used to calculate the angle of orientation of the transition moment instead of the molecular axis.

DISCUSSION

There are two possible mechanisms for the translocation of buforin 2. The peptide may cross lipid bilayers in a similar way to magainin 2, i.e., via the transient formation of a peptide−lipid supramolecular complex (toroidal) pore, but the extremely short lifetime of the pore does not allow detectable dye leakage and lipid flip-flop. There is an inverse relationship between pore stability and translocation efficiency because translocation occurs only upon disintegration of the pore (*35*). Alternatively, buforin 2 may translocate by a novel mechanism.

The translocation efficiencies of BF2 and MG2 were similarly dependent on the peptide concentrations (Figure 1), suggesting the translocation mechanisms are similar. A comparable dependence on concentration was observed for the ion channel formation of magainin 2 (*36*). The cooperativity of pore formation is often interpreted as due to peptide aggregation; however, a new model based on the elasticity of membrane has been recently proposed (*37*, *38*). The incorporation of the negative curvature-inducing lipid EYPE completely suppressed the translocation of BF2, indicating the induction of a positive curvature by BF2 on the membrane is related to the translocation process, similarly to MG2 (*11*). The significant increase in the fraction of the hydrated carbonyl group from 71% (spectra not shown) to 89 and 85% (Figure 4) in the presence of BF2 and MG2, respectively, may also be a consequence of a peptide-induced expansion of the headgroup region of the membrane, i.e., positive curvature. These data support a magainin-like translocation mechanism. The lifetime of a toroidal pore, which is modulated by electrostatic interactions, is expected to depend on not only peptide charge (*35*) but also lipid charge, because the pore is composed of peptides and lipids. Neither significant leakage nor lipid flip-flop was observed in EYPG/EYPC (1:1) bilayers (*16*), whereas in pure EYPG, where the repulsion between polycationic BF2 molecules in a small pore is reduced, dye leakage and coupling lipid flip-flop were clearly observed (Figure 2), corroborating the hypothesis that the translocation mechanism of BF2 is essentially the same as that of MG2.

The Pro^{11} residue plays a key role in effective translocation (*16*, *39*). The unique structure of proline is known to allow the cis−trans isomerization of the amide bond. The observation that buforin 2 does not exist as a single conformation in 50% trifluoroethanol (*40*) may be related to this property. Our experiments clearly showed that the isomerization is not involved in the translocation process (Figure 3). Another unique property of proline is that it induces a kink in an α-helix. In the case of buforin 2, this residue causes a distortion of the helix. The NMR study in 50% trifluoroethanol revealed that in one of the highly populated states, buforin 2 assumes a regular α-helix between residues Val^{12} and Arg^{20} and a distorted helical structure between residues Gly^7 and Pro^{11} and that this unusual helical structure extends the amphipathic region to the residues Arg^5−Lys^{21}(*40*). The structure of BF2 in lipid bilayers must be similar to this structure, because the CD spectrum of the peptide in this solvent mixture was superimposable to that in EYPG/EYPC vesicles (*16*). The larger half-width of the BF2 amide I′ band (23 cm^{-1}) compared to that of MG2 (band 3, 15 cm^{-1}) is in agreement with the heterogeneity of the helical structure (Figure 4). The longer amphipathic region of BF2 compared to that of P11A-BF2 is reflected in the higher affinity of BF2 for EYPG/EYPC bilayers (Figure 1A). The slightly greater concentration dependence of P11A-BF2 translocation (Figure 1C) may indicate that larger amounts of the peptide must be accumulated to induce the positive curvature necessary for toroidal pore formation. The apparent smaller orientational angle of the BF2 helix than that of the MG2 helix (Table 1), which essentially lies parallel to the membrane surface at lower P/L values (*8*, *9*, *41*), may also be a consequence of the helical distortion.

In conclusion, BF2 translocates across lipid bilayers by a mechanism similar to that of MG2. The presence of Pro^{11} makes the Arg^5−Lys^{21} region amphipathic by distoring the helix. Five positive charges clustered on this 17-residue sequence extremely destabilize a pore in EYPG/EYPC bilayers, enabling the peptide to translocate effectively

without causing dye leakage and lipid flip-flop. This local positive charge density of BF2 is higher than that of F12W, E19Q-magainin 2 amide having five positive charges on 23 residues which already has significantly reduced leakage activity and enhanced translocation activity compared to MG2 (*35*). In EYPG bilayers with a higher negative charge density, the peptide−lipid supramolecular complex pore is electrostatically stabilized. Therefore, dye leakage and lipid flip-flop are detectable, and translocation efficiency is reduced. The flip-flop-to-leakage ratio in this lipid system (Figure 2) was larger than that in the EYPG/EYPC system (*16*), indicating a smaller pore in EYPG bilayers (*12*). A reduction in interpeptide repulsion appears to diminish the pore size.

REFERENCES

1. Lehrer, R. I., and Ganz, T. (1999) Antimicrobial peptides in mammalian and insect host defence, *Curr. Opin. Immunol. 11*, 23−27.
2. Hancock, R. E., and Scott, M. G. (2000) The role of antimicrobial peptides in animal defenses, *Proc. Natl. Acad. Sci. U.S.A. 97*, 8856−8861.
3. Zasloff, M. (2002) Antimicrobial peptides of multicellular organisms, *Nature 415*, 389−395.
4. Yeaman, M. R., and Yount, N. Y. (2003) Mechanisms of antimicrobial peptide action and resistance, *Pharmacol. Rev. 55*, 27−55.
5. Zasloff, M. (1987) Magainins, a class of zntimicrobial peptides from *Xenopus* skin: Isolation, characterization of two active forms, and partial cDNA sequene of a precursor, *Proc. Natl. Acad. Sci. U.S.A. 84*, 5449−5453.
6. Matsuzaki, K. (1998) Magainins as paradigm for the mode of action of pore forming polypeptides, *Biochim. Biophys. Acta 1376*, 391−400.
7. Matsuzaki, K. (1999) Why and how are peptide-lipid interactions utilized for self-defence? Magainins and tachyplesins as archetypes, *Biochim. Biophys. Acta 1462*, 1−10.
8. Bechinger, B., Zasloff, M., and Opella, S. J. (1993) Structure and orientation of the antibiotic peptide magainin in membranes by solid-state nuclear magnetic resonance spectroscopy, *Protein Sci. 2*, 2077−2084.
9. Matsuzaki, K., Murase, O., Tokuda, H., Funakoshi, S., Fujii, N., and Miyajima, K. (1994) Orientational and aggregational states of magainin 2 in phospholipid bilayers, *Biochemistry 33*, 3342−3349.
10. Wieprecht, T., Dathe, M., Epand, R. M., Beyermann, M., Krause, E., Maloy, W. L., MacDonald, D. L., and Bienert, M. (1997) Influence of the angle subtended by the positively charged helix face on the membrane activity of amphipathic, antimicrobial peptides, *Biochemistry 36*, 12869−12880.
11. Matsuzaki, K., Sugishita, K., Ishibe, N., Ueha, M., Nakata, S., Miyajima, K., and Epand, R. M. (1998) Relationship of membrane curvature to the formation of pores by magainin, *Biochemistry 37*, 11856−11863.
12. Matsuzaki, K., Murase, O., Fujii, N., and Miyajima, K. (1996) An antimicrobial peptide, magainin 2, induced rapid flip-flop of phospholipids coupled with pore formation and peptide translocation, *Biochemistry 35*, 11361−11368.
13. Ludtke, S. J., He, K., Heller, W. T., Harroun, T. A., Yang, L., and Huang, H. W. (1996) Membrane pores induced by magainin, *Biochemistry 35*, 13723−13728.
14. Matsuzaki, K., Murase, O., Fujii, N., and Miyajima, K. (1995) Translocation of a channel-forming antimicrobial peptide, magainin 2, across lipid bilayers by forming a pore, *Biochemistry 34*, 6521−6526.
15. Park, C. B., Kim, M. S., and Kim, S. C. (1996) A novel antimicrobial peptides from *Bufo bufo gargarizans*, *Biochem. Biophys. Res. Commun. 218*, 408−413.
16. Kobayashi, S., Takeshima, K., Park, C. B., Kim, S. C., and Matsuzaki, K. (2000) Interactions of the novel antimicrobial peptide buforin 2 with lipid bilayers: proline as a translocation promoting factor, *Biochemistry 39*, 8648−8654.
17. Park, C. B., Kim, H. S., and Kim, S. C. (1998) Mechanism of action of the antimicrobial peptide buforin ii: buforin ii kills microorganisms by penetrating the cell membrane and inhibiting cellular functions, *Biochem. Biophys. Res. Commun. 244*, 253−257.
18. Takeshima, K., Chikushi, A., Lee, K.-K., Yonehara, S., and Matsuzaki, K. (2003) Translocation of analogues of the antimicrobial peptides magainin and buforin across human cell membranes, *J. Biol. Chem. 278*, 1310−1315.
19. Bartlett, G. R. (1959) Phosphorus assay in column chromatography, *J. Biol. Chem. 234*, 466−468.
20. Ladokhin, A. S., Wimley, W. C., and White, S. H. (1995) Leakage of membrane vesicle contents: determination of mechanism using fluorescence requenching, *Biophys. J.*, 1964−1971.
21. Goormaghtigh, E., Raussens, V., and Ruysschaert, J.-M. (1999) Attenuated total reflection infrared spectroscopy of proteins and lipids in biological membranes, *Biochim. Biophys. Acta 1422*, 105−185.
22. Matsuzaki, K., Shioyama, T., Okamura, E., Umemura, J., Takenaka, T., Takaishi, Y., Fujita, T., and Miyajima, K. (1991) A comparative study on interactions of α-aminoisobutyric acid containing antibiotic peptides, trichopolyn I and hypelcin A with phosphatidylcholine bilayers, *Biochim. Biophys. Acta 1070*, 419−428.
23. Uematsu, N., and Matsuzaki, K. (2000) Polar angle as a determinant of amphipathic α-helix-lipid interactions: a model peptide study, *Biophys. J. 79*, 2075−2083.
24. Creighton, T. E. (1993) in *Proteins, Structures and Molecular Properties* Chapter 1, W. H. Freeman and Company, New York.
25. Delaney, N. G., and Madison, V. (1982) Novel conformational distributions of methylproline peptides, *J. Am. Chem. Soc. 104*, 6635−6641.
26. Hinds, M. G., Welsh, J. H., Brennand, D. M., Fisher, J., Glennie, M. J., Richards, N. G. J., Turner, D. L., and Robinson, J. A. (1991) Synthesis, conformational properties, and antibody recognition of peptides containing β-turn mimetics based on α-alkylproline derivatives, *J. Med. Chem. 34*, 1777−1789.
27. Tong, Y., Olczak, J., Zabrocki, J., Gershengorn, M. C., Marshall, G. R., and Moeller, K. D. (2000) Constrained peptidomimetics for TRH: cis-Peptide bond analogues, *Tetrahedron 56*, 9791−9800.
28. Blume, A., Huebner, W., and Messner, G. (1988) Fourier transform infrared spectroscopy of $^{13}C{=}O$-labeled phospholipids hydrogen bonding to carbonyl groups, *Biochemistry 27*, 8239−8249.
29. Ter-Minassian-Saraga, L., Okamura, E., Umemura, J., and Takenaka, T. (1988) Fourier transform infrared-attenuated total reflection spectroscopy of hydration of dimyristoylphosphatidylcholine multibilayers, *Biochim. Biophys. Acta 946*, 417−423.
30. Chirgradze, Y. N., Fedorov, O. V., and Trushina, N. P. (1975) Estimation of amino acid residue side chain absorption in the infrared spectra of protein solutions in heavy water, *Biopolymers 14*, 679−694.
31. Tatulian, S. A. (2003) Attenuated total reflection Fourier transform infrared spectroscopy: A method of choice for studying membrane proteins and lipids, *Biochemistry 42*, 11898−11907.
32. Jackson, M., Mantsch, H. H., and Spencer, J. (1992) Conformation of magainin 2 and related peptide in aqueous solution and membrane environments probed by Fourier transform infrared spectroscopy, *Biochemistry 31*, 7289−7293.
33. Yano, Y., Takemoto, T., Kobayashi, S., Yasui, H., Sakurai, H., Ohashi, W., Niwa, M., Futaki, S., Sugiura, Y., and Matsuzaki, K. (2002) Topological stability and self-association of a completely hydrophobic model transmembrane helix in lipid bilayers, *Biochemistry 41*, 3073−3080.
34. Fraser, R. D. B., and MacRae, T. P. (1973) *Conformation in Fibrous Proteins and Related Polypeptides*, Academic Press, New York.
35. Matsuzaki, K., Nakamura, A., Murase, O., Sugishita, K., Fujii, N., and Miyajima, K. (1997) Modulation of magainin 2-lipid bilayer interactions by peptide charge, *Biochemistry 36*, 2104−2111.
36. Cruciani, R. C., Barker, J. L., Durell, S. R., Raghunathan, G., Guy, H. R., Zasloff, M., and Stanley, E. F. (1992) Magainin 2, a natural antibiotic from frog skin, forms ion channels in lipid bilayer membranes, *Eur. J. Pharmacol., Mol. Pharmacol. Sect. 226*, 287−296.
37. Chen, F.-Y., Lee, M.-T., and Huang, H. W. (2002) Sigmoidal concentration dependence of antimicrobial peptide activities: a case study on alamethicin, *Biophys. J. 82*, 908−914.

38. Lee, M.-T., Chen, F.-Y., and Huang, H. W. (2004) Energetics of pore formation induced by membrane active peptides, *Biochemistry 43*, 3590−3599.
39. Park, C. B., Yi, K.-S., Matsuzaki, K., Kim, M. S., and Kim, S. C. (2000) Structure−activity analysis of buforin II, a histone H2A-derived antimicrobial peptide: The proline hinge is responsible for the cell-penetrating ability of buforin II, *Proc. Natl. Acad. Sci., U.S.A. 97*, 8245−8250.
40. Yi, G.-S., Park, C. B., Kim, S. C., and Cheong, C. (1996) Solution structure of an antimicrobial peptide buforin II, *FEBS Lett. 398*, 87−90.
41. Ludtke, S. J., He, K., Wu, Y., and Huang, H. W. (1994) Cooperative membrane insertion of magainin correlated with its cytolytic activity, *Biochim. Biophys. Acta 1190*, 181−184.

BI048206Q